INSTITUTE OF PHYSICS PUBLISHING JOURNAL OF OPTICS A: PURE AND APPLIED OPTICS

J. Opt. A: Pure Appl. Opt. **8** (2006) S122–S130 doi:10.1088/1464-4258/8/4/S11

Negative index meta-materials based on two-dimensional metallic structures

Gennady Shvets[1] **and Yaroslav A Urzhumov**

Physics Department, The University of Texas at Austin, Austin, TX 78712, USA

E-mail: gena@physics.utexas.edu

Received 30 August 2005, accepted for publication 17 October 2005
Published 22 March 2006
Online at stacks.iop.org/JOptA/8/S122

Abstract

The electromagnetic properties of two-dimensional metallic nanostructures in the optical frequency range are studied. One example of such a structure is a periodic array of thin metallic strip pairs. The magnetic response of these structures is studied, as is the closely related emergence of the negative index of refraction propagation bands. The presence of such bands is found to critically depend on the proximity of electric and magnetic dipole resonances. It is demonstrated that the frequencies of those resonances are strongly dependent on the ratio of the structure thickness and the plasmonic skin depth. Electromagnetic structures that are much thicker than the plasmonic skin depth are shown to exhibit standard broad antenna resonances at the wavelength roughly twice the strip length. As the structures are scaled down to resonate in the visible/mid-infrared, electrostatic resonances determine the electromagnetic properties of such materials.

Keywords: negative index materials, optical magnetism, metamaterials

(Some figures in this article are in colour only in the electronic version)

1. Introduction and motivation

Meta-materials is a general term referring to man-made composites which have the desirable properties unavailable in the naturally occurring materials. Extending the range of materials' *electromagnetic* properties is currently the main driving force behind the development of meta-materials. For example, it has recently been demonstrated that meta-materials containing split ring resonators can have a negative magnetic permeability $\mu < 0$ in the microwave [1] and even terahertz [2] frequency ranges. When additional elements, such as continuous conducting wires [3], are introduced into an elementary cell of a meta-material, both the dielectric permittivity and magnetic permeability can be made negative [4]. Such negative index materials (NIMs) with $\varepsilon < 0$ and $\mu < 0$ are particularly promising because of the possibility of making a 'perfect' lens with sub-wavelength spatial resolution [5]. NIMs can be very useful for many other microwave and optical applications [6–10] as well.

Developing NIMs for optical frequencies, however, has proven to be challenging. Although there are naturally occurring materials (metals, polaritonic materials such as SiC, ZnSe, MnO in mid-infrared) with a negative ϵ, using the scaled-down version of the original split-ring resonator is more challenging due to fabrication issues. For example, the original double split ring concept [1] was replaced by the simplified single split ring resonator (SRR) [11] to demonstrate magnetic response in the infrared part of the spectrum. Even further simplifications of the unit cell may be necessary to develop magnetic response at near-infrared/visible frequencies. As the resonant structures are simplified, there is less opportunity for increasing their capacitance and inductance by making their aspect ratios (e.g., ratio of the SRR's radius and gap size) high. Hence, increasing the ratio of the resonant wavelength λ to the cell periodicity L becomes more difficult. It is the high λ/L ratio that distinguishes a true meta-material from its more common cousin, the photonic crystal [13, 14].

Another limitation of the split-ring resonator was recently recognized: because it does not have an inversion symmetry, electromagnetic resonances cannot be classified as purely electric dipole or magnetic dipole resonances. Consequently,

[1] Author to whom any correspondence should be addressed.

both electric and magnetic responses are strongly excited at the same frequency unless significant modifications of the structure [12] are made. Therefore, it can be difficult to experimentally distinguish between the two. This was experimentally demonstrated at infrared frequencies [11] by exciting the magnetic resonance of a split ring in the illumination geometry that had the incident and induced magnetic fields orthogonal to each other. This property of non-centrosymmetric structures is known as bi-anisotropy. Electromagnetic wave propagation in bi-anisotropic structures is substantially different than that in NIMs [12]. On the other hand, electromagnetic modes of centrosymmetric structures can be classified according to their spatial symmetry as electric dipolar, electric quadrupolar, magnetic dipolar, etc. Thus, one can identify frequency ranges where the structure has either electric or magnetic response.

In order to realize NIMs at high (optical) frequencies, there is a need to consider electromagnetic materials with the unit cell satisfying the following conditions:

(a) fabrication simplicity,
(b) inversion symmetry (to avoid bi-anisotropy),
(c) availability of both magnetic and electric resonances in close frequency proximity of each other, and
(d) small elementary cell size compared to the wavelength.

We will consider the simplest metallic structures, metallic strip pairs, and demonstrate using numerical simulations how the negative index property emerges from electric and magnetic resonances. We will show how sub-wavelength infrared resonances of these structures naturally occur as the structures become thinner. These resonances are electrostatic in nature, and their resonant frequency is determined by the shape of the structure and the frequency-dependent dielectric permittivity of the metal. The transition from geometric resonances (dependent on both the shape and the size of the structure) to plasmonic (electrostatic) resonances (shape-dependent, size-independent) occurs when the smallest dimension of the structure becomes smaller than the skin depth.

2. Negative index meta-materials based on perfectly conducting strip pairs

The concept of a resonance is fundamental to understanding and designing meta-materials. This is especially true when very exotic electromagnetic properties of a meta-material are desired, such as, for example, a negative magnetic permeability. For example, the approximate formula for the magnetic permeability of a meta-material consisting of SRRs [1] reads

$$\mu_{\mathrm{eff}} = 1 - \frac{F\omega^2}{\omega^2 - \omega_{\mathrm{M}}^2 + \mathrm{i}\omega\Gamma}, \qquad (1)$$

where F is the fractional area of a unit cell occupied by the SRR, ω_{M} is the magnetic resonance frequency, and Γ is the resistive loss coefficient. The filling factor F is typically kept small to avoid strong interaction between adjacent unit cells. Therefore, $\mu_{\mathrm{eff}}(\omega) < 0$ only for ωs in the close vicinity of the magnetic resonance frequency ω_{M}. A similar expression [15]

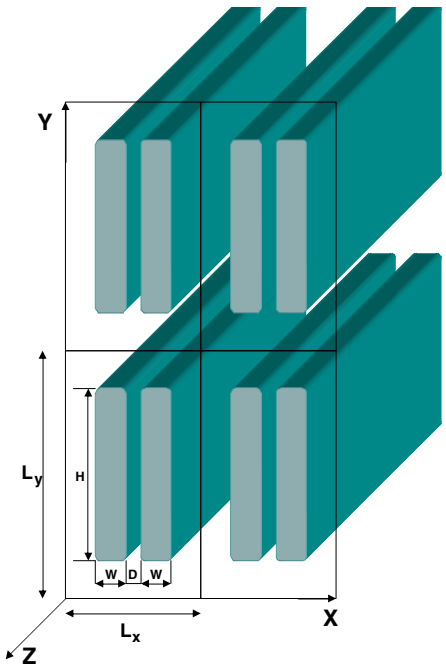

Figure 1. Two horizontally spaced layers of vertically stacked pairs of metallic strips. The layers are infinitely extended in the y-direction with periodicity L_y. The separation between strips is D, and the height and width of each strip is H and W, respectively.

exists for a periodic meta-material consisting of wire elements into which cuts are periodically introduced:

$$\epsilon_{\mathrm{eff}} = 1 - \frac{\omega_{\mathrm{p}}^2 - \omega_{\mathrm{E}}^2}{\omega^2 - \omega_{\mathrm{E}}^2 + \mathrm{i}\omega\Gamma}, \qquad (2)$$

where ω_{p} is the characteristic 'plasma' frequency and ω_{E} is the cut-wire resonance frequency. Except for a very specific and often practically challenging case of uninterrupted wires ($\omega_{\mathrm{E}} = 0$), negative ϵ_{eff} exists in the immediate proximity of the electric resonance at $\omega = \omega_{\mathrm{E}}$. Thus it can be argued that developing a NIM may require finding a resonant structure that has adjacent electric and magnetic resonances.

Luckily, the simplest structure exhibiting nearby resonances consists of two thin metallic strips placed next to each other. Two horizontally spaced layers of such metallic strips (vertically stacked on top of each other) is shown in figure 1. For computational simplicity and to facilitate qualitative understanding, the strips are assumed to be infinitely extended in the z-direction. All calculations below assume that the fields are not varying in the z-direction as well. A P-polarized electromagnetic wave with nonvanishing E_x, E_y, and H_z field components incident on the layer can excite both electric and magnetic resonances. Because no resonances are expected to be excited by the S-polarized electromagnetic wave, our calculations are restricted to P-polarization.

Magnetic resonance is excited because the magnetic field H_z of the incident wave is normal to the plane of the strip pair. The double-strip structure has centre of inversion symmetry. This symmetry ensures that the structure is not bi-anisotropic: electric and magnetic resonances occur at different frequencies. The magnetic resonance can thus only

be excited by the magnetic field perpendicular to x–y plane. It cannot be excited by the electric field alone (with magnetic field in the x–y plane) as is the case with bi-anisotropic structures [16, 17]. In any case, the assumption of field invariance along the z-direction precludes us from modelling such a case.

To determine and characterize possible resonances of a perfectly conducting metallic strip pair (MSP), we have numerically calculated the transmission coefficient $T(\omega)$ of a P-polarized electromagnetic wave normally incident on a single layer of vertically stacked MSPs as a function of the incident wave frequency ω. MSP layer geometry is defined by the following parameters: $H/L_y = 0.64$, $W = D = H/8$. Here L defines the spatial scale, and L_y is the periodicity in the y-direction. The simulation was done using the commercial finite elements code FEMLAB [18] that solves a two-dimensional *fixed frequency* Helmholtz equation for the magnetic field H_z:

$$-\nabla^2 H_z = \frac{\omega^2}{c^2} H_z, \tag{3}$$

where the following boundary conditions are satisfied:

(a) $\partial_n H_z = 0$ at the metal surface (here ∂_n is the normal derivative),
(b) $\partial_x H_z + \mathrm{i}\omega H_z/c = 2\mathrm{i}\omega H_0$ at $x = -L_\mathrm{B}$, and
(c) $\partial_x H_z - \mathrm{i}\omega H_z/c = 0$ at $x = L_\mathrm{B}$.

Here ∂_n is the normal derivative at the metal surface, H_0 is the amplitude of the electromagnetic wave incident on the structure from the left, and $x = \pm L_\mathrm{B}$ are the computational domain boundaries. Boundary condition (c) corresponds to the source-free radiative boundary condition. Boundary condition (b) corresponds to the radiative boundary condition with an external source. For all simulations $\omega < 2\pi c/L$, making the single-layer structure a sub-wavelength diffraction grating. The computational domain was chosen large enough so that the evanescent diffractive orders are negligibly small: $L_\mathrm{B} = 5L$.

The assumption that a MSP is a perfect conductor is accurate only when the strip thickness W is much larger than the skin depth of the incident light. For most metals this translates into $W \gg 20$ nm for infrared frequencies. Most recently reported experimental results (see, for example, [11]) on detecting magnetic response in the infrared do indeed fall under the 'perfect conductor' category. The plot of $T(\omega)$ shown in figure 2 (top) exhibits two pronounced transmission dips. The first dip at $\omega L/c \equiv \omega_\mathrm{E}^{(1)} L/c \approx 2.7$ is very broad and relatively shallow. Plotting the field structure (electric and magnetic fields) at that frequency reveals its electric dipole nature: the bottom (top) caps of both metallic strips are positively (negatively) charged. The magnetic field between the strips is essentially zero because the electric current in both strips flows in the same direction.

The high-frequency dip at $\omega L/c \approx 4.6$ is narrow and deep: transmission reduces to numerically undetectable level. Note that this dip occurs when $H/\lambda \approx 0.44$ (where $\lambda = 2\pi c/\omega$ is the light wavelength), corresponding to the well-known half-wavelength antenna resonance. The structure of the fields is, however, much more complicated at that frequency than at the $\omega_\mathrm{E}^{(1)}$ frequency. To understand the structure of the fields better, a leaky mode analysis (LMA) was developed. LMA

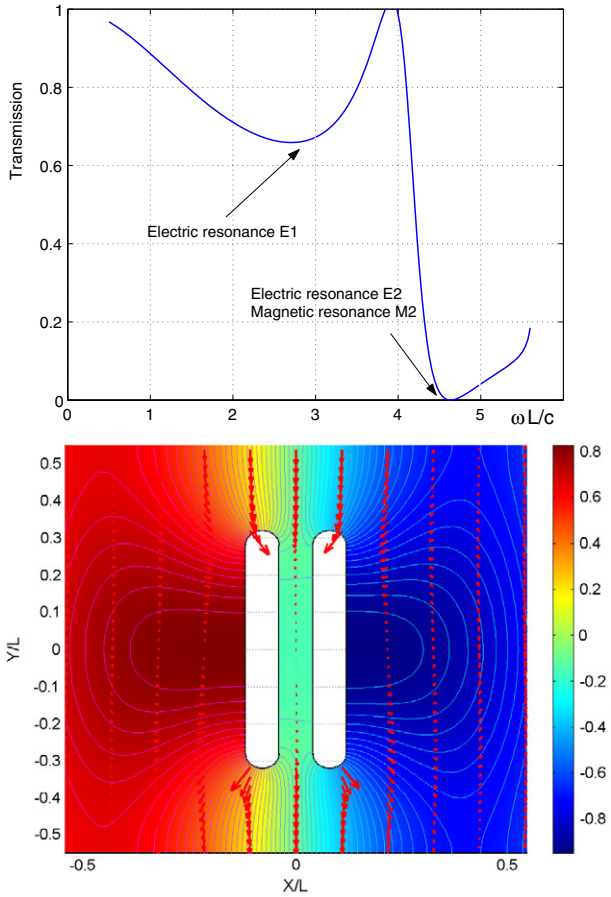

Figure 2. Top: transmission coefficient through a single (in the x-direction) layer of perfectly conducting metallic strip pairs (MSPs) shown in figure 1. MSP parameters: $L_y = L$, $H/L = 0.64$, $W = D = H/8$. The two transmission dips correspond to the excitation of a broad electric dipole resonance E1 (at $\omega_\mathrm{E}^{(1)} L/c \approx 2.7$) and closely spaced electric and magnetic dipole resonances E2 and M2 (at $\omega_{E,M}^{(2)} L/c \approx 4.6$). Bottom: electric field (arrows) and magnetic field isocontours corresponding to $\omega_\mathrm{E}^{(1)}$.

enables us to extract resonances of the structure by assuming that the electromagnetic field concentrated in the vicinity of the structure is weakly coupled to the outgoing radiative mode. By imposing the source-free radiative boundary conditions at $x = \pm L_\mathrm{B}$ (where $L_\mathrm{B} \gg L$), the complex frequencies $\omega \equiv \omega_\mathrm{r} - \mathrm{i}\omega_\mathrm{i}$ of the leaky modes can be extracted. Radiative losses are characterized by ω_i while the real mode frequency is ω_r.

2.1. Magnetic and electric resonances of metallic strips: leaky mode analysis

The natural frequencies of the leaky modes of a single layer of MSPs are found by solving equation (3) as an eigenvalue equation for a complex frequency $\omega \equiv \omega_\mathrm{r} - \mathrm{i}\omega_\mathrm{i}$, subject to the source-free radiative boundary conditions. Only weakly leaking modes with $\omega_\mathrm{i} \ll \omega_\mathrm{r}$ were studied. Specifically, the following boundary conditions have been imposed: $\partial_x H_z + \mathrm{i}\omega_\mathrm{r} H_z/c = 0$ at $x = -L_\mathrm{B}$ and $\partial_x H_z - \mathrm{i}\omega_\mathrm{r} H_z/c = 0$ at $x = L_\mathrm{B}$. Because the boundary conditions are dependent

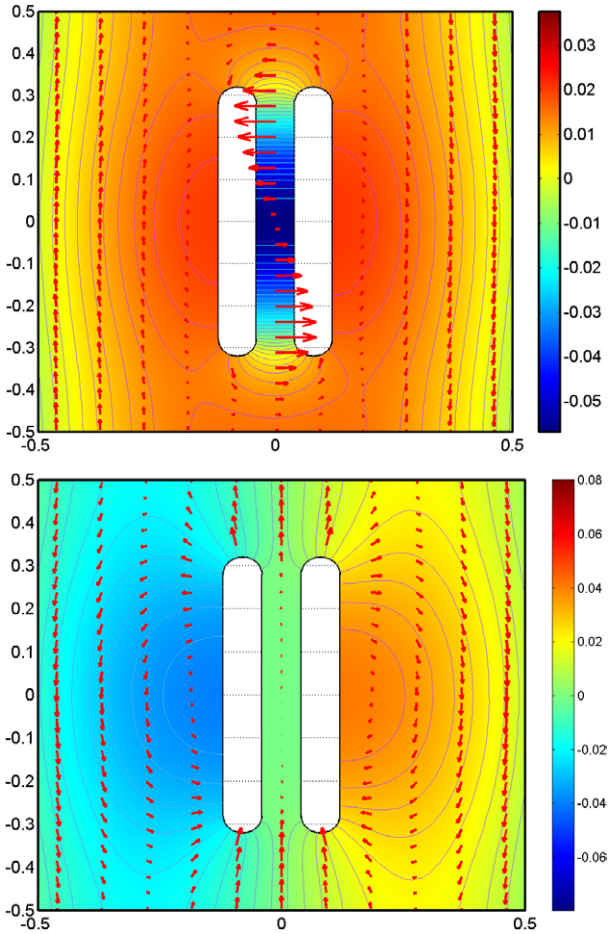

Figure 3. Leaky mode profiles corresponding to the magnetic dipole resonance at $\omega_{\mathrm{M}}^{(2)}L/c = 4.68 - 0.43\mathrm{i}$ (top) and $\omega_{\mathrm{E}}^{(2)}L/c = 4.73 - 0.49\mathrm{i}$ (bottom). The MSP geometry is the same as in figure 2. The electric field strength and direction are shown by proportionate arrows. Isocontours and colouring correspond to the magnetic field.

on the frequency of the leaky mode we are seeking by solving the eigenvalue equation (3) for ω, we have used an iterative procedure. First, a trial $\omega_{\mathrm{r}}^{(1)}$ is chosen and the complex eigenvalue $\omega^{(1)}$ is obtained. Then the real part of $\omega^{(1)}$ is chosen as $\omega_{\mathrm{r}}^{(2)}$, and the process is repeated until convergence is reached after N iterations: $\mathrm{Re}(\omega^{(N)}) = \omega_{\mathrm{r}}^{(N)}$. The iterative sequence typically converged after fewer than ten iterations.

The numerically computed eigenfrequencies are $\omega_{\mathrm{M}}^{(2)}L/c = 4.68 - 0.43\mathrm{i}$ and $\omega_{\mathrm{E}}^{(2)}L/c = 4.73 - 0.49\mathrm{i}$. Their identification as magnetic and electric dipole resonances, respectively, is done by inspecting electric and magnetic field profiles of the respective eigenmodes shown in figure 3. The field structure of the electric dipole resonance in the bottom figure 3 is the same as in figure 2 (bottom), and is identified as the electric dipole resonance. The field distribution corresponding to $\omega = \omega_{\mathrm{M}}^{(2)}$ shown in the top figure 3 is qualitatively different. Inspection of the charge distribution on the metal surface indicates that the electric dipole moment of the MSP is equal to zero. That is because the charge distribution possesses an inversion symmetry. However, the quadrupole electric moment and the magnetic dipole moment

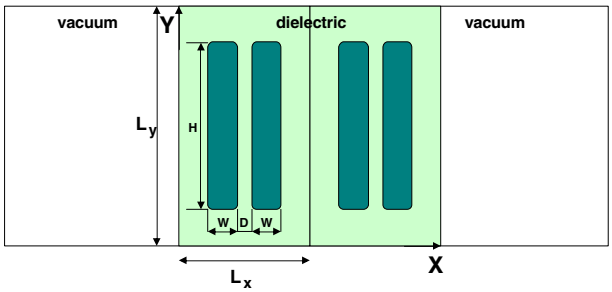

Figure 4. Two horizontal layers of vertically stacked pairs of metallic strips embedded in a dielectric with $\epsilon_{\mathrm{d}} = 4$. Layers are infinitely extended in the y-direction with periodicity L_y. Geometric parameters: $L_x = 0.64L$, $L_y = 0.8L$, $H/L = 0.64$, $W = D = H/8$.

are not vanishing. The latter is finite because the currents are flowing in the opposite direction in the two MSP-forming strips. The nonvanishing of the magnetic moment can also be seen in figure 3 (top) by inspecting a strong enhancement of the magnetic field in the region between the metallic strips.

Two important lessons can be learned from this single-layer LMA. First, it confirms that the electric and magnetic resonances occur at different frequencies due to the inversion symmetry of the MSP. Second, this example illustrates that, while the frequencies of the two resonances are not identical, they do occur in a relatively close proximity of each other. Therefore, one can expect that there is a finite frequency interval where both $\epsilon_{\mathrm{eff}} < 0$ and $\mu_{\mathrm{eff}} < 0$ for a (multilayer) structure infinitely extended in both the x- and y-directions. An important downside of the MSP-based design of a NIM is that the resulting meta-material is not strongly sub-wavelength: $L/\lambda \approx 0.75$ at the magnetic resonance. That is due to the extreme simplicity of the MSP structure: none of the capacitance-increasing techniques used in the design of an SRR [1] have been employed here. On the other hand, the simplicity of the MSP structure makes it attractive for deployment as a building block of a visible/near-IR NIM. The structure can be made sub-wavelength due to the emergence of the plasmonic resonances as the strip width W becomes smaller. This approach to miniaturization of the unit cell to the sub-λ level is described in section 3.1.

2.2. Negative index material based on embedded metallic strip pairs

A sub-wavelength negative index meta-material can be designed by embedding metallic strip pairs in a high-ϵ dielectric and taking advantage of the proximity of the electric and magnetic resonances demonstrated in section 2.1. Specifically, we model a NIM consisting of periodically repeated MSPs, with horizontal and vertical periods $L_x = 0.64L$ and $L_y = 0.8L$. A sketch is given in figure 4. Here L is a geometric scale of the meta-material in terms of which its parameters (periodicity, the shape of its constituent MSP) are expressed. MSPs are assumed to be embedded in a high dielectric permittivity material with $\epsilon_{\mathrm{d}} = 4$. Embedding MSPs in a dielectric serves two goals: (i) lowering the resonant frequency by approximately $\sqrt{\epsilon_{\mathrm{d}}}$, and (ii) defining a sharp clearly defined interface between the vacuum and the NIM. The

effective impedance $Z_{\rm eff}(\omega)$ and refractive index $n_{\rm eff}(\omega)$ can be extracted from the reflection and transmission coefficients $r(\omega)$ and $t(\omega)$ through a slab of thus constructed meta-material with thickness Δ [19, 20]:

$$Z_{\rm eff}(\omega) = \pm\sqrt{\frac{t^2-(1-r)^2}{t^2-(1+r)^2}}, \tag{4}$$

$$n_{\rm eff}(\omega) = \frac{\ln Y(\omega)}{{\rm i}\omega\Delta/c}, \tag{5}$$

where

$$X \equiv \cos(n_{\rm eff}\omega\Delta/c) = (1-r^2+t^2)/(2t), \tag{6}$$

$$Y \equiv {\rm e}^{{\rm i}n_{\rm eff}\omega\Delta/c} = X \pm \sqrt{X^2-1}. \tag{7}$$

The signs in expressions (4) and (7) are chosen such that the conditions ${\rm Re}(Z_{\rm eff}) > 0$ and ${\rm Im}(n_{\rm eff}) > 0$ are satisfied [20].

The transmission/reflection coefficients $t(\omega)$ and $r(\omega)$ are *complex* numbers containing both the phase and amplitude information (unlike the transmission amplitude $T \equiv |t|^2$ plotted in figure 2 (top) for a single layer of MSPs in vacuum). We have used the standard approach developed earlier [19, 20] for extracting an unambiguous refractive index by varying the slab thickness. In our case, varying $\Delta \equiv NL$ is equivalent to varying the number of elementary unit layers N. This number is varied from $N_{\rm min} \geqslant 1$ to $N_{\rm max} > N_{\rm min}$ with unit increment, so that the phase ϕ_N of the complex exponent in equation (7) for N layers does not change by more than π when one switches from N layers to $N+1$. In photonic crystals, this assumption always holds, because the x-component of the Bloch wavenumber $k_{\rm Bloch} \equiv n_{\rm eff}\omega/c$ cannot exceed π/L_x in magnitude, so that $|k_{\rm Bloch}L_x| \leqslant \pi$, and thus the phase $\phi_N = k_{\rm Bloch}NL_x + \psi_0$ cannot change by more than π. This property of periodic structures allows one to eliminate phase jumps greater than π and to draw a smooth, nearly linear curve ϕ_N versus N. This curve is used to extract ψ_0. After subtraction of $\phi_c = 2\pi[\psi_0/(2\pi)]$ from ϕ_N (brackets denote rounding to nearest integer) each point of the curve $\phi_N - \phi_c$ represents the actual value of $n_{\rm eff}(N)N\omega L_x/c$, where $n_{\rm eff}$ is the effective refraction index of the structure with N layers. If all $n_{\rm eff}(N)$ are approximately the same, the meta-material behaves as a homogeneous effective medium. This assumption has been tested and found to be satisfied for all structures described here.

The effective dielectric permittivity and magnetic permeability are related to $Z_{\rm eff}$ and $n_{\rm eff}$ as $\epsilon_{\rm eff} = n_{\rm eff}/Z_{\rm eff}$ and $\mu_{\rm eff} = n_{\rm eff}Z_{\rm eff}$. Numerically extracted $\epsilon_{\rm eff}$ and $\mu_{\rm eff}$ are plotted in figure 5. Reflection and transmission coefficients were obtained for an electromagnetic wave incident along the x-direction on a meta-material slab. Therefore, the extracted $\epsilon_{\rm eff}$ is the ε_{yy} component of the effective dielectric permeability tensor ε. Because the structure is clearly anisotropic (the x- and y-directions are not equivalent), only wave propagation in the x-direction is considered. The negative index is exhibited only along that direction.

From figure 5 (top) it follows that the extracted values of $\epsilon_{\rm eff}$ and $\mu_{\rm eff}$ of such a meta-material are both negative in the vicinity of $\omega = 2c/L$. Therefore, this meta-material is expected to support electromagnetic waves with

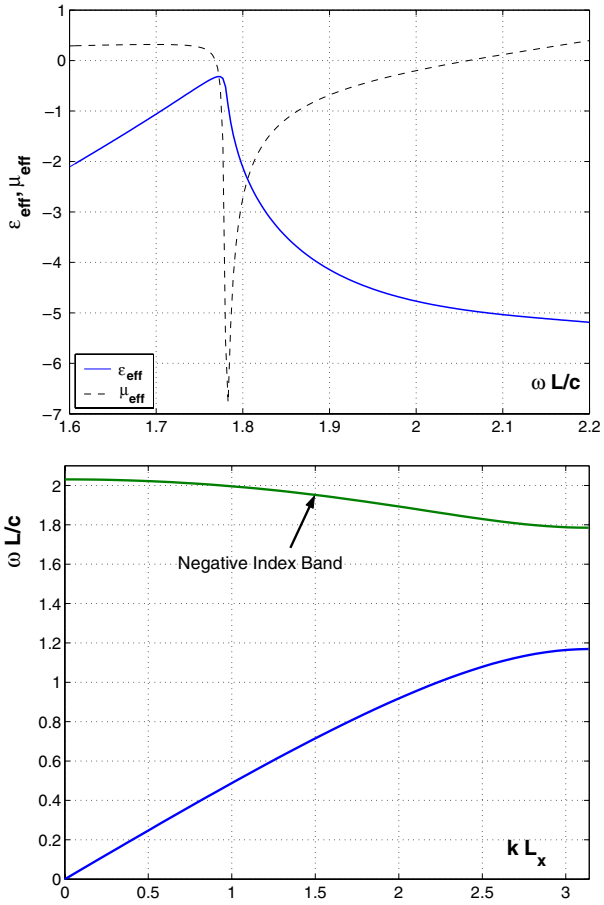

Figure 5. Top: extracted dielectric permittivity ϵ and magnetic permeability $\mu_{\rm eff}$ for a NIM consisting of a square lattice of metallic strip pairs (MSPs) embedded in a $\epsilon_{\rm d} = 4$ dielectric. Bottom: band diagram ω versus k exhibiting a negative index band. The wave vector $\vec{k} = k\vec{e}_x$ is directed along x-direction. MSP geometric parameters: $L_x = 0.64L$, $L_y = 0.8L$, $H/L = 0.64$, $W = D = H/8$.

a negative refractive index. To demonstrate the presence of a negative index band, the band structure of the meta-material was calculated by imposing phase-shifted periodic boundary conditions [21] at the left and right cell boundaries: $H_z(x=0,y) = \exp({\rm i}kL_x)H_z(x=L_x,y)$ and $\partial_x H_z(x=0,y) = \exp({\rm i}kL_x)\partial_x H_z(x=L_x,y)$. The wavenumber k satisfies the $0 < k < \pi/L_x$ condition. Solving equation (3) as an eigenvalue equation for ω yields the dispersion curve ω versus k plotted in figure 5 (bottom). The second propagation band indeed has a negative refractive index because its group velocity opposes its phase velocity: $\partial\omega/\partial k < 0$.

One drawback of the present NIM design is that the unit cell of this meta-material is only marginally sub-wavelength: $L_x/\lambda = 0.2$. Even this modest miniaturization of a unit cell is accomplished by embedding the MSPs in a high-ϵ material. While such materials can be found in the near- and mid-infrared (for example, $\epsilon_{\rm Si} = 12$), they are less common in the visible. The solutions of equation (3), with perfectly conducting boundary conditions at the metal surface, are *scalable*, i.e. determined by a single dimensionless parameter $\omega L/c$ for a given geometry of the MSP layer. Therefore,

making a strongly sub-wavelength MSP-based NIM in the optical range is as hard (or harder, given the absence of suitable high-ϵ dielectrics) as in the microwave range. A different approach must be used. One such approach described below is to take advantage of the *plasmonic* resonances of an MSP.

3. Plasmonic resonances of ultrathin pairs of metallic strips

The concept of using electrostatic resonances for inducing optical magnetism was recently [21–23] introduced by us. In those papers electrostatic resonances of periodic plasmonic nanostructures have been employed to induce magnetic properties due to the close proximity of adjacent nanowires. Higher multipole electrostatic resonances were shown [23] to hybridize in such a way as to induce magnetic moments in individual nanowires. Strong electrostatic resonances of regularly shaped nanoparticles (including nanospheres and nanowires) occur for $-2 < \epsilon_R < -1$, where $\epsilon_m(\omega) \equiv \epsilon_R(\omega) + i\epsilon_I(\omega)$ is the frequency-dependent dielectric permeability of the metal from which the MSP is made.

The drawback of such designs [21, 22] is that if metal is used in such a meta-material, negative index is found only for the frequencies at which resistive damping is high: if $-2 < \epsilon_R < -1$, then ϵ_I is comparable to ϵ_R. Qualitatively, this occurs because of interband transitions in metals. Moving away from interband transitions (and corresponding high losses) requires reducing the frequency ω and, therefore, increasing the absolute value of $\epsilon_R(\omega)$. Making the structures resonate at the frequency ω such that $\epsilon_R(\omega) \ll -1$ requires moving from simple shapes (cylinder, sphere, etc) to more complicated geometric shapes characterized by extreme aspect ratio values. For example, it is known [24] that gold nanoshells with a dielectric core/metall shell structure resonate at a much lower frequency than pure gold nanoparticles if the thickness of the gold shell is much smaller than the core radius. As demonstrated below, the MSPs shown in figure 1 exhibit electrostatic resonances for $\epsilon_R \ll -1$ if $H \gg W, D$.

The fundamental wave equation that must be solved for the magnetic field H_z is

$$-\vec{\nabla} \cdot \left(\frac{1}{\epsilon} \vec{\nabla} H_z \right) = \frac{\omega^2}{c^2} H_z, \tag{8}$$

where $\epsilon(x, y, \omega)$ is a frequency and position-dependent function: $\epsilon \equiv \epsilon_m(\omega)$ inside the metallic strips and $\epsilon \equiv 1$ outside the strips. Here $\epsilon_m(\omega)$ is the material-dependent dielectric permittivity. For most metals $\epsilon_m = 1 - \omega_p^2/\omega(\omega + i\Gamma)$ is a good approximation obtained on the basis of the Drude model. Below we use material constants typical for many metals (but specific to Au): $c/\omega_p = 23$ nm and $\Gamma/\omega_p = 3 \times 10^{-3}$. Equation (8) replaces (3) which assumed that a metal is a perfect conductor. Both equations give the same result if the skin depth $l_{sk} \sim c/\omega_p$ is much smaller than the metal thickness W.

We refer to metallic structures with characteristic thickness $W \leqslant c/\omega_p$ as *plasmonic*. An array of plasmonic MSPs presents a very different medium to an incident electromagnetic wave than an array of perfectly conducting MSPs described in section 2. Because of the dependence of

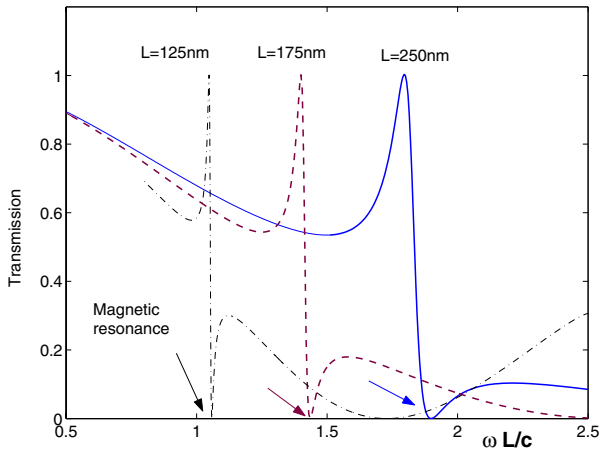

Figure 6. Frequency dependence of the transmission coefficient through a single layer of plasmonic MSPs spaced in vacuum by $L_y = 0.8L$. Geometric parameters of the MSP: $H/L = 0.64$, $W = D = H/8$. Solid line: $L = 250$ nm, dashed line: $L = 175$ nm, dot–dashed line: $L = 125$ nm.

ϵ_m on the frequency, these structures are no longer scalable, unlike the perfectly conducting MSPs. For example, if the transmission coefficient $T_0 = T(\omega_0)$ through the layer of MSPs is observed for a characteristic structure size L_0, then one cannot expect that $T(S\omega_0) = T_0$ for a scaled-down structure with a characteristic size $L = L_0/S$. Scalability of perfectly conducting MSPs presents a serious disadvantage for making a sub-wavelength NIM: no matter how small the unit cell is, NIM behaviour is observed at a proportionally short wavelength. The question posed by us here is: does the lack of scaling for realistic (plasmonic) MSPs at the optical frequencies enable a sub-wavelength NIM, or does it make the structures disproportionately large? Below we demonstrate that the lack of simple scaling enables sub-wavelength meta-materials. However, the same MSP-based design that reveals negative index behaviour when the unit cell is large (and the wavelength long) may not reveal such behaviour for scaled-down unit cells.

To investigate the lack of scalability in plasmonic structures we simulated transmission through a single layer of MSPs spaced in vacuum by $L_y = 0.8L$. For three different structures with $L = 250$, 175, and 125 nm the transmission coefficient is plotted in figure 6 as a function of the dimensionless parameter $\omega L/c$. The same perfectly matched boundary conditions at $x = \pm L_B$ and periodic boundary conditions at $y = \pm L_y/2$ were applied as in the simulations described in section 2. The difference is that equation (8) is solved instead of equation (3) and that a finite-permittivity material with $\epsilon_m(\omega)$ is assumed inside the MSPs instead of a perfect conductor. For this simulation we have neglected the very small damping constant $\Gamma \ll \omega$. Two important differences between the perfectly conducting and plasmonic case are apparent when comparing any one of the three curves in figure 6 to figure 2 (top). First, the transmission dips (magnetic dipole resonances) in the plasmonic case are much sharper. We have verified that the dips indeed correspond to the excitation of magnetic resonances by inspecting the magnetic field distribution. Indeed, the magnetic field is

strongly concentrated inside the MSP, as shown in figure 3 (top). Second, the normalized frequencies corresponding to the magnetic resonance are smaller in the plasmonic case: $\omega_{\rm M}^{(2)} L/c \approx 1.05$ for the $L = 125$ nm plasmonic case versus $\omega_{\rm M}^{(2)} L/c = 4.7$ for the perfectly conducting case. Because resistive damping is neglected in our plasmonic simulations, the sharpness of the resonance is indeed related to the lower normalized frequency: optically small objects with $L \ll \lambda$ experience low radiative damping.

Comparison between the three curves in figure 6 also shows that thinner structures are more sub-wavelength. This proves that the plasmonic structures are not scalable. In fact, reducing the scale size of the structure by a factor 2 (from $L = 250$ to 125 nm) reduces the normalized resonance frequency $\omega_{\rm M}^{(2)} L/c$ by an almost equal factor. This implies that as the structures become very small, the resonant wavelength reaches a certain saturation value. Miniaturizing the structures further makes them progressively more sub-wavelength. Therefore, the non-scalability of the magnetic resonances of plasmonic MSPs is *advantageous* for designing sub-wavelength meta-materials.

It is instructive to note that the widths of the MSPs in the three cases shown in figure 6 are, in descending order, $W = 20, 15, 10$ nm. Therefore, all three MSPs are thinner than the skin depth $l_{\rm sk} \sim c/\omega_{\rm p} = 23$ nm. It is in this regime of ultrathin metallic structures that the electrostatic effects are expected to become prominent. To demonstrate that plasmonic effects indeed become dominant for the three structure sizes considered here, it is instructive to calculate the real values of $\epsilon_{\rm m}(\omega_{\rm M}^{(2)})$ at the magnetic resonance frequencies. Those are: $\epsilon_{\rm m} = -31$ for $L = 250$ nm, $\epsilon_{\rm m} = -27$ for $L = 175$ nm, and $\epsilon_{\rm m} = -25$ for $L = 125$ nm. Evidently, as the structures shrink, the $\epsilon_{\rm m}$ reaches some fixed value. This effect is consistent with the observation that shrinking the structure size does not affect the resonant frequency. Below, the magnetic resonance in sub-wavelength MSPs is shown to be electrostatic in origin.

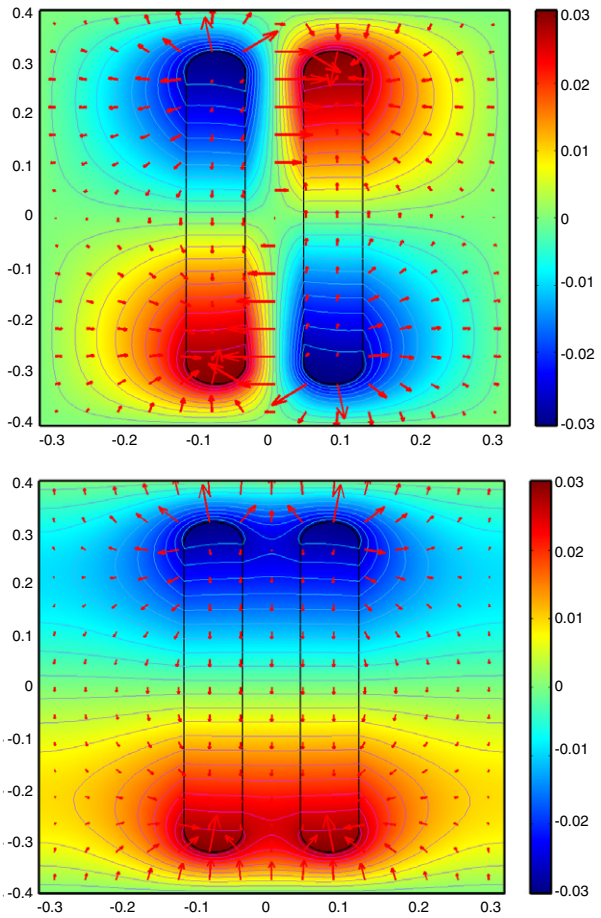

Figure 7. Top: magnetic resonance at $\epsilon_1 = -22.75$, bottom: electric resonance at $\epsilon_2 = -9.9$. Contours: lines of equal potential $\Phi_{\rm i}$. Resonances are computed for a periodic meta-material with $L_x = 0.64L$, $L_y = 0.8L$, $H/L = 0.64$, $W = D = H/8$.

3.1. Electrostatic nature of plasmonic resonances

In the limit of $\omega L/c \ll 1$ the right-hand side of equation (8) representing the retardation effects can be neglected, yielding $\vec{\nabla} \cdot (\epsilon^{-1} \vec{\nabla} H_z) = 0$. This equation is equivalent [22, 23] to assuming that the electric field is purely electrostatic: $\vec{E} \equiv \vec{E}_{\rm ES}$, $\vec{\nabla} \times \vec{E}_{\rm ES} = 0$, or $\vec{E}_{\rm ES} = -\vec{\nabla}\Phi$, where Φ is the electrostatic potential. The Poisson equation in the medium satisfied by Φ is

$$\vec{\nabla} \cdot \left(\epsilon \vec{\nabla} \Phi \right) = 0, \tag{9}$$

where, as in equation (8), $\epsilon \equiv \epsilon(x, y, \omega)$ is a function of space. Equation (9) can be solved as a generalized eigenvalue equation (GEE) for the frequencies of electrostatic resonances $\omega_{\rm i}$. This is equivalent to solving a GEE for $\epsilon_{\rm i} \equiv \epsilon_{\rm m}(\omega_{\rm i})$ because the frequency only enters equation (9) through the dielectric permittivity. Using the fact that $\epsilon(x, y)$ is a piecewise continuous function that assumes only two values, equation (9) can be recast [25, 26] as

$$\vec{\nabla} \cdot \left[\theta(\vec{x}) \vec{\nabla} \Phi_{\rm i} \right] = s_{\rm i} \nabla^2 \Phi_{\rm i}, \tag{10}$$

where $\phi_{\rm i}$ are the potential functions corresponding to electrostatic resonances, and $s_{\rm i} \equiv 1/(1 - \epsilon_{\rm i})$ is a generalized eigenvalue. For a lossless plasmonic material the expression for $s_{\rm i}$ is particularly simple: $s_{\rm i} = \omega_{\rm i}^2/\omega_{\rm p}^2$. Thus, small values of $s_{\rm i}$ correspond to low frequencies and large negative values of the corresponding $\epsilon_{\rm m}(\omega_{\rm i})$.

Bearing in mind that we are interested in describing the y-polarized wave propagation in a periodic structure, $\Phi_{\rm i}(y = \pm L_y/2) = 0$ and $\Phi_{\rm i}(x = -L_x/2) = \Phi_{\rm i}(x = L_x/2)$ boundary conditions [23] were used. The finite elements code FEMLAB [18] was used to solve equation (10). The resonances thus obtained can be classified according to the symmetry of the potential function Φ with respect to symmetry group transformations of the unit cell. For example, the electric quadrupole resonance shown in figure 7 (top) corresponding to $s_1 = 0.042$ (or $\epsilon_1 \equiv \epsilon_{\rm EQ} = -22.75$) is even with respect to spatial inversion and odd with respect to mirror reflections in the y–z and x–z planes. The electric dipole resonance shown in figure 7 (bottom) has an odd inversion symmetry, and odd (even) mirror symmetry with respect to reflection in x–z (y–z) planes. This resonance occurs at $s_2 = 0.09$ (or $\epsilon_2 \equiv \epsilon_{\rm ED} = -9.9$). As was earlier demonstrated [22], resonances with such spatial symmetry contribute to the quasi-static dielectric permittivity ε_{yy}. Electric dipole resonant frequency $\omega_{\rm ED}$ corresponds to divergent (or very large, in the case of finite resistive losses) dielectric permittivity. This is

easy to see by inspecting the potential distribution in figure 7 (bottom). The potential difference between $y = +L_y/2$ and $y = -L_y/2$ planes is equal to zero. However, the electric field flux through those planes (which is proportional to the electric charge) is finite. Therefore, the capacitance of such a capacitor and, correspondingly, the effective dielectric permittivity, are infinite. The electric quadrupole resonance at the lower frequency ω_{EQ} does not contribute to the dielectric permittivity. But, as shown below, when small but finite retardation effects are retained, this resonance acquires a magnetic dipole component.

These simulation results highlight yet another important property of plasmonic strip pairs: electrostatic resonances occur at the frequencies corresponding to a large negative value of ϵ_m. This is an important distinction from the electrostatic resonances at $\epsilon_m \sim -1$ of regularly shaped (circular [22] or triangular [21]) plasmonic structures studied by us earlier: large values of $|\epsilon_m|$ occur at lower frequencies where absorption due to interband transitions is small.

An important finding of the electrostatic analysis is that electric and magnetic dipole resonances occur at rather different wavelengths. This is in sharp contrast to the case of perfectly conducting MSPs, where the two resonances are at very close frequencies. The assumption of perfect conductivity is valid only for the structures that are much thicker than the skin depth: $W \gg \lambda_{sk}$. Using the above example of an ultrathin structure and the tabulated values of ϵ_m for gold, it is found that the electric quadrupole (and the magnetic dipole related to it) resonance occurs at $\lambda = 770$ nm, while the electric dipole resonance is at $\lambda = 590$ nm. This large difference results in the disappearance of the negative index band in the miniaturized MSP-based structure. Thus, even though an MSP-based meta-material with a large unit cell can exhibit a NIM band as shown in figure 5 (bottom), a scaled-down structure does not necessarily support such a band.

3.2. Magnetic moment at the electric quadrupole resonance

It is rather remarkable that the frequency ω_{EQ} of the electric quadrupole resonance calculated by simulating our system in the electrostatic approximation corresponds to $\epsilon_m = -22.75$. As was shown in section 3.1, the magnetic resonance moves from $\epsilon_m = -31$ for $L = 250$ nm to $\epsilon_m = -27$ for $L = 175$ nm, and to $\epsilon_m = -25$ for $L = 125$ nm as the MSPs are getting progressively smaller. These values are remarkably close to $\epsilon_m(\omega_{EQ})$ at the electric quadrupole resonance frequency, suggesting that there is a natural connection between the two. Below we demonstrate that, indeed, the electric quadrupole acquires a finite magnetic moment when the retardation effect (finite value of $\omega L/c$) is accounted for. A somewhat related effect was described for a U-shaped nano-antenna using a different approach [27].

We start by separating the total magnetic and electric fields into $H_z = H_{qs} + H_1$ and $\vec{E} = \vec{E}_{ES} + \vec{S}$, where $\vec{E}_{ES} = \mathrm{i}c\epsilon^{-1}\vec{\nabla} \times \vec{H}_{qs}/\omega$ and $\vec{S} = \mathrm{i}c\epsilon^{-1}\vec{\nabla} \times \vec{H}_1/\omega$. Physically, this separation means that the electric field is divided into electrostatic ($\vec{E}_{ES} = -\vec{\nabla}\Phi$) and solenoidal ($\vec{\nabla} \cdot \vec{S} = 0$) parts. The magnetic field is split up into quasi-static (H_{qs} satisfying $\vec{\nabla} \cdot (\epsilon^{-1}\vec{\nabla}H_{qs}) = 0$) and electromagnetic ($H_1$) parts. The quasi-static magnetic field is small, of order $\omega L/c$, compared with the electrostatic electric field: $|H_{qs}| \sim (\omega L/c)|\vec{E}_{ES}|$. The electromagnetic component H_1 satisfies, to order $\omega^2 L^2/c^2$, the following equation:

$$\vec{\nabla} \cdot \left(\frac{1}{\epsilon}\vec{\nabla}H_1\right) = \frac{\omega^2}{c^2}H_{qs}. \tag{11}$$

Therefore, H_1 is even smaller that H_{qs}: $|H_1| \sim \omega^2 L^2/c^2|H_{qs}|$. Therefore, H_1 is neglected in what follows. The magnetic field $\vec{H}_{qs} = \vec{e}_z H_{qs}$ can be calculated from $\vec{\nabla} \times \vec{H}_{qs} = -\mathrm{i}\omega\epsilon\vec{E}_{ES}/c$. The peak amplitude of the magnetic field $|H_{qs}|$ can be evaluated by noting that, from $\vec{\nabla} \times \vec{E}_{ES} = 0$, the vertical component of the electrostatic field E_y inside the metal strips is related to the peak horizontal electric field E_x at the caps of the strips through $|E_y| = |E_x|D/H$. Therefore, $|H_{qs}| \sim (\omega W D/cH)|\epsilon_m||E_x|$. Thus, $|H_{qs}| \ll |E_x|$ because $W \ll H$, $D \ll H$, and, by assumption, $\omega H/c < 1$.

The effective magnetic permeability of a meta-material differs from unity due to induced magnetic moments. The electric current pattern through the MSPs at the quadrupole resonance is clearly such that the currents flow in opposite directions through the adjacent strips. It would be a mistake, however, to assume that the entire current contributes to the generation of the magnetic moment. In determining the contribution of the induced electric current in the MSP to the magnetic moment, it is essential to keep in mind that the current pattern contains both the magnetic dipole and electric quadrupole [28]. The quadrupole part originates from the electrostatic field and does not contribute to the magnetic moment. The magnetic dipole portion of the current originates from the solenoidal component of the electric field $\vec{S}$ that can be calculated [23] from H_{qs}:

$$\vec{\nabla} \times \vec{S} = \mathrm{i}\frac{\omega}{c}H_{qs}\vec{e}_z, \tag{12}$$

and $\vec{\nabla} \cdot \vec{S} = 0$. The magnitude of $\vec{S}$ inside the strips is estimated as $|\vec{S}| \sim (\omega W/c)|\bar{H}_{qs}|$, where $|\bar{H}_{qs}|$ is the peak value of H_{qs} between the strips. The magnetic moment density is given by $\vec{M} = (1/2c)\langle\vec{r} \times \vec{J}_S\rangle$, where $\vec{J}_S = -\mathrm{i}\omega(\epsilon_m - 1)\vec{S}$ represents the solenoidal component of the electric field and the $\langle\cdots\rangle$ stands for averaging over the unit cell. For the MSP it is estimated that $|\vec{M}| \sim p|\epsilon_m - 1|(\omega^2 W D/c^2)|\bar{H}_{qs}|$, where $p = 2WH/(L_x L_y)$ is the fractional area of the unit cell occupied by the MSPs. This qualitative estimate highlights the fact that magnetic properties of plasmonic nanostructures are indeed proportional to the retardation effects and, therefore, scale as the square of the frequency.

4. Conclusions

The electromagnetic properties of two-dimensional meta-materials consisting of an array of metallic strips pairs (MSPs) are investigated using electromagnetic simulations. Simulated transmission through a single layer of MSPs show that electromagnetic resonances corresponding to electric and magnetic dipole resonances can be excited. Large MSPs such that the strip thickness significantly exceeds the skin depth can be modelled as perfect conductors. Perfectly conducting MSPs are shown to possess electric and magnetic dipole resonances which are very close in frequency. This property

of MSPs is used to demonstrate a sub-wavelength negative index meta-material based on MSPs. These resonances are related to the well-known antenna resonances occurring at the wavelength approximately equal to twice the strip height H. A new approach to making a strongly sub-wavelength MSP-based meta-material is demonstrated. This approach involves reducing the size of the unit cell to the point at which plasmonic (electrostatic) resonances of MSPs become dominant. Two types of electrostatic resonance, dipole and quadrupole, are investigated. The quadrupole resonance is shown to contribute to the magnetic moment of the meta-material and, therefore, to result in the optical magnetism.

Acknowledgments

This work was supported by the ARO MURI grant W911NF-04-01-0203 and by the DARPA contract HR0011-05-C-0068.

References

[1] Pendry J B, Holden A J, Robbins D J and Stewart W J 1999 *IEEE Trans. Microw. Theory Technol.* **47** 2075
[2] Yen T J, Padilla W J, Fang N, Vier D C, Smith D R, Pendry J B, Basov D N and Zhang X 2004 *Science* **203** 1494
[3] Pendry J B, Holden A J, Stewart W J and Youngs I 1996 *Phys. Rev. Lett.* **76** 4773
[4] Smith D R, Padilla W J, Vier D C, Nemat-Nasser S C and Schultz S 2000 *Phys. Rev. Lett.* **84** 4184
[5] Pendry J B 2000 *Phys. Rev. Lett.* **85** 3966
[6] Parazzoli C G, Greegor R B, Li K, Koltenbah B E C and Tanielian M 2003 *Phys. Rev. Lett.* **90** 107401
[7] Caloz C and Itoh T 2003 *IEEE Microw. Wireless Comp. Lett.* **13** 547
[8] Horii Y, Caloz C and Itoh T 2005 *IEEE Trans. Microw. Theory Technol.* **53** 1527
[9] Alu A and Engheta N 2004 *IEEE Trans. Microw. Theory* **52** 199
[10] Podolskiy V A and Narimanov E E 2005 *Phys. Rev.* B **71** 201101
[11] Linden S, Enkrich C, Wegener M, Zhou J, Koschny T and Soukoulis C M 2004 *Science* **306** 1351
[12] Marques R, Medina F and Rafii-El-Idrissi R 2002 *Phys. Rev.* B **65** 144440
[13] Yablonovich E 1987 *Phys. Rev. Lett.* **58** 2059
[14] John S 1987 *Phys. Rev. Lett.* **58** 2486
[15] Pendry J B and Smith D R 2004 *Phys. Today* **57** 37
[16] Gay-Balmaz P and Martin O J F 2002 *J. Appl. Phys.* **92** 2929
[17] Katsarakis N, Koschny T, Kafesaki M, Economou E N and Soukoulis C M 2004 *Appl. Phys. Lett.* **84** 2943
[18] FEMLAB Reference Manual 2003 Version 2.3 Comsol AB, Sweden
[19] Smith D R, Schultz S, Markos P and Soukoulis C M 2002 *Phys. Rev.* B **65** 195104
[20] Markos P and Soukoulis C M 2003 *Opt. Express* **11** 649
[21] Shvets G 2003 *Phys. Rev.* B **67** 035109
[22] Shvets G and Urzhumov Y A 2004 *Phys. Rev. Lett.* **93** 243902
[23] Shvets G and Urzhumov Y A 2005 *J. Opt. A: Pure Appl. Opt.* **7** S23
[24] Nordlander P, Prodan E, Radloff C and Halas N J 2003 *Science* **302** 419
[25] Bergman D J and Stroud D 1992 *Solid State Phys.* **46** 147
[26] Stockman M I, Faleev S V and Bergman D J 2001 *Phys. Rev. Lett.* **87** 167401
[27] Sarychev A K and Shalaev V M 2004 *Proc. SPIE* **5508** 128
[28] Vinogradov A P and Aivazyan A V 1999 *Phys. Rev.* B **60** 987